Downloaded from orbit.dtu.dk on: May 03, 2024

DTU Library

Remarkable conductivity enhancement in P-doped polythiophenes via rational engineering of polymer-dopant interactions

Kim, Jongho; Guo, Jing; Sini, Gjergji; Sørensen, Michael Korning; Andreasen, Jens Wenzel; Woon, Kai Lin; Coropceanu, Veaceslav; Paleti, Sri Harish Kumar; Wei, Huan; Peralta, Sébastien

Total number of authors:
15

Published in:
Materials Today Advances

Link to article, DOI:
10.1016/j.mtadv.2023.100360

Publication date:
2023

Document Version
Publisher's PDF, also known as Version of record

Link back to DTU Orbit

Citation (APA):
Kim, J., Guo, J., Sini, G., Sørensen, M. K., Andreasen, J. W., Woon, K. L., Coropceanu, V., Paleti, S. H. K., Wei, H., Peralta, S., Mallouki, M., Müller, C., Hu, Y., Bui, T. T., & Wang, S. (2023). Remarkable conductivity enhancement in P-doped polythiophenes via rational engineering of polymer-dopant interactions. *Materials Today Advances*, *18*, Article 100360. https://doi.org/10.1016/j.mtadv.2023.100360

General rights
Copyright and moral rights for the publications made accessible in the public portal are retained by the authors and/or other copyright owners and it is a condition of accessing publications that users recognise and abide by the legal requirements associated with these rights.

- Users may download and print one copy of any publication from the public portal for the purpose of private study or research.
- You may not further distribute the material or use it for any profit-making activity or commercial gain
- You may freely distribute the URL identifying the publication in the public portal

If you believe that this document breaches copyright please contact us providing details, and we will remove access to the work immediately and investigate your claim.

Materials Today Advances 18 (2023) 100360

Contents lists available at ScienceDirect

Materials Today Advances

journal homepage: www.journals.elsevier.com/materials-today-advances/

Remarkable conductivity enhancement in P-doped polythiophenes via rational engineering of polymer-dopant interactions

Jongho Kim [a], Jing Guo [b], Gjergji Sini [a,*], Michael Korning Sørensen [c], Jens Wenzel Andreasen [c], Kai Lin Woon [d], Veaceslav Coropceanu [e], Sri Harish Kumar Paleti [f], Huan Wei [b], Sébastien Peralta [a], Mohamed Mallouki [a], Christian Müller [f], Yuanyuan Hu [b,**], Thanh-Tuan Bui [a], Suhao Wang [a,***]

[a] Laboratoire de Physicochimie des Polymères et des Interfaces, CY Cergy Paris Université, 5 Mail Gay Lussac, 95000, Neuville-sur-Oise, France
[b] Changsha Semiconductor Technology and Application Innovation Research Institute & International Science and Technology Innovation Cooperation Base for Advanced Display Technologies of Hunan Province, College of Semiconductors (College of Integrated Circuits), Hunan University, Changsha, 410082, China
[c] Department of Energy Conversion and Storage, Technical University of Denmark, 2800, Kgs. Lyngby, Denmark
[d] Low Dimensional Material Research Center, Department of Physics, University Malaya, Kuala Lumpur, 50603, Malaysia
[e] Department of Chemistry and Biochemistry, The University of Arizona, Tucson, AZ, 85721-0088, USA
[f] Department of Chemistry and Chemical Engineering, Chalmers University of Technology, 41296, Göteborg, Sweden

ARTICLE INFO

Article history:
Received 14 December 2022
Received in revised form
28 February 2023
Accepted 2 March 2023
Available online xxx

Keywords:
Conducting polymers
Charge-transport
Doping
Aggregations
DFT calculations

ABSTRACT

Molecular doping is an effective approach to tune the charge density and optimize electrical performance of conjugated polymers. However, the introduction of dopants, on the other hand, may disturb the polymer microstructure and disrupt the charge transport path, often leading to a decrease of charge carrier mobility and deterioration of electrical conductivity of the doped films. Here we show that dopant-induced disorder can be overcome by rational engineering of polymer-dopant interactions, resulting in remarkable enhancement of electrical conductivity. Benchmark poly(3-hexylthiophene) (P3HT) and its analogous random polymers of 3-hexylthiophene and thiophene P[$(3HT)_{1-x}$-stat-$(T)_x$] were synthesized and doped by 2,3,5,6-tetrafluoro-7,7,8,8-tetracyanoquinodimethane (F4TCNQ). Remarkably, random P[$(3HT)_{1-x}$-stat-$(T)_x$] was doped to a far superior electrical conductivity, that in the case of $x \geq 0.24$, the conductivity of P[$(3HT)_{1-x}$-stat-$(T)_x$] is over 100 times higher than that of the doped P3HT, despite both P3HT and P[$(3HT)_{1-x}$-stat-$(T)_x$] exhibit comparable charge carrier mobility in their pristine state and in spite of their practically identical redox properties. This result can be traced back to the formation of π-stacked polymer-dopant-polymer co-crystals exhibiting extremely short packing distances of 3.13–3.15 Å. The mechanism behind these performances is based on a new role played by the dopant molecules that we name "bridging-gluing". The results are coherently verified by the combination of optical absorption spectroscopy, X-ray diffraction, density functional theory calculations, and molecular dynamics simulations.
© 2023 The Author(s). Published by Elsevier Ltd. This is an open access article under the CC BY-NC-ND license (http://creativecommons.org/licenses/by-nc-nd/4.0/).

1. Introduction

Conjugated polymers have been extensively investigated as promising materials in various (opto)electronic devices because of their excellent semiconducting properties and advantages over their inorganic counterparts, including mechanical flexibility and solution processability [1–6]. Doping of organic semiconductors has recently emerged as a powerful strategy to enhance the performance of these devices [7]. Thanks to its ability of reducing Ohmic losses and passivating trap states, molecular doping has been recognized as an enabler for organic light-emitting diodes (OLEDs) [8–10], organic solar cells (OSCs) [11,12], and organic field effect transistors (OFETs) [13–17]. Moreover, molecular doping also allows for tuning the charge density and optimizing the

* Corresponding author.
** Corresponding author.
*** Corresponding author.
E-mail addresses: gjergji.sini@cyu.fr (G. Sini), yhu@hnu.edu.cn (Y. Hu), suhao.wang1@cyu.fr (S. Wang).

https://doi.org/10.1016/j.mtadv.2023.100360
2590-0498/© 2023 The Author(s). Published by Elsevier Ltd. This is an open access article under the CC BY-NC-ND license (http://creativecommons.org/licenses/by-nc-nd/4.0/).

performance of thermoelectric polymers as well as energy storing redox polymers [18–22]. Nevertheless, there has been a long-lasting challenge that the introduction of dopants often inevitably disturbs polymer film microstructure, especially for the most intensively studied benchmark semicrystalline polymer P3HT, resulting in decreased charge carrier mobility and an unfavorable reduction in electrical conductivity. For instance, P3HT typically exhibits electrical conductivities up to 0.02–1 S cm^{-1} when doped with electron acceptor F4TCNQ by mixed-solution doping method [23–26]. The conductivity values of doped P3HT are mainly limited by the disorder-sensitive behavior of P3HT. Specifically, as previously reported, regioregularity has a significant impact on the semiconducting charge transport properties of P3HT, such that the pristine regioregular (RR) P3HT films exhibited a highly ordered molecular packing and a remarkable charge carrier mobility that is over four orders of magnitude higher than its pristine regiorandom (RRa) counterpart which lacked long-range order [27,28]. Consequently, after doping with F4TCNQ, RR-P3HT showed electrical conductivities that are ca. 3 orders of magnitude higher than that of RRa-P3HT [29,30]. After introducing dopants into P3HT films by mixed-solution processing method, the film morphology was disrupted, leading to decreased charge carrier mobility [31]. It is worth noting that in the case of RRa-P3HT, although the dopants were observed to induce ordering of the amorphous region [30,32], the ultimate electrical conductivity of doped RRa-P3HT is still significantly lower than that of the doped RR-P3HT, mainly due to the fact that RRa-P3HT lacks the ability to aggregate and adopt ordered conformations which allows hole charges to delocalize after initially contacting with the dopant [33].

To reduce the disruption of dopants on the microstructure of host polymers, sequential doping (i.e., spin coating layers of dopants on top of pre-deposited polymer films) has been employed to dope conjugated polymers leading to less disrupted film microstructures and improved electrical conductivity [34–39]. It is observed that F4TCNQ molecules mainly located in the amorphous region in the P3HT film after sequential doping, increasing conjugation length of the amorphous chains as well as the film connectivity [39]. However, for organic electronic devices requiring thick film depositions, sequential doping may face limitations in bulk doping. Besides, vapor-phase sublimation approach has also been used to diffuse dopants into polymer films resulting in undisturbed film microstructures and higher electrical performance [29,40–42], yet the doping level is often hard to be accurately controlled by this method. Since solution processing is considered as future process for organic electronic devices, especially considering that mix-solution doping is a straightforward one-step solution processing method, it is thus of vital importance to enhance the resilience of conjugated polymers to dopant-induced disorder during mix-solution processing such that their electrical conductivity can be improved to higher levels upon doping.

Promisingly, the emerging molecular designing strategy for disorder-resilient conjugated polymers may offer an effective solution [43–50]. The emerging conjugated polymers are typically featured with pronounced short-range order in the form of aggregates [51,52], enabling them to maintain decent charge carrier mobilities even when their film microstructures lack long-range order as detected by X-ray diffraction technique. Taking the n-type benchmark polymer P(NDI2OD-T2) as an example, the regioirregular (RI) version of the polymer exhibited decent charge carrier mobilities that are only a few times lower than its RR counterpart [53]. When doped, RI-P(NDI2OD-T2) exhibited comparable or even higher conductivity values than that of RR-P(NDI2OD-T2) [54,55], in striking contrast to the difference between RR-P3HT and RRa-P3HT. When confined within an inert polymer matrix, the X-ray diffraction feature along both π-stacking and alkyl stacking directions of the P(NDI2OD-T2) films was completely crushed, but the blended films still maintained similar local aggregation feature to that of the pure semiconductor film [56], resulting in undisturbed charge transport behavior. Nevertheless, enhancing tolerance to disorder in the doped conjugated polymers is scarcely reported.

Here we propose and verify a strategy to enhance the resilience of conjugated polymers to dopant-induced disorder by rational engineering polymer-dopant interactions. P3HT and its three analogous random polymers, P[$(3HT)_{0.88}$-stat-$(T)_{0.12}$], P[$(3HT)_{0.76}$-stat-$(T)_{0.24}$], and P[$(3HT)_{0.64}$-stat-$(T)_{0.36}$] were synthesized and doped by F4TCNQ with mix-solution doping method (Fig. 1). It is expected that polymer—F4TCNQ—polymer co-crystals can be formed when T content reaches a certain level, leading to ordered macrostructure instead of disordered structure. We show that even though the charge carrier mobilities of all the four pristine polymers are comparable, P[$(3HT)_{0.76}$-stat-$(T)_{0.24}$] and P[$(3HT)_{0.64}$-stat-$(T)_{0.36}$] can be doped to reach electrical conductivities that are over 2 orders of magnitude higher than that of the doped P3HT. Importantly, we observed that these random polymers interacted with dopants to form pronounced long-range order, thus resulting in significantly improved electrical conductivities. Remarkably, as an emerging efficient hole-transporting unit, the formation of polymer-dopant-polymer sandwich supramolecular system (co-crystals) through a "bridging-gluing" effect with extremely tight packing distance of 3.13 Å was recognized accountable for the high conductivity observed for P[$(3HT)_{0.76}$-stat-$(T)_{0.24}$] and P[$(3HT)_{0.64}$-stat-$(T)_{0.36}$]. These results were corroborated by supporting characterizations such as electron spin resonance (ESR), UV–vis–NIR, and Grazing Incidence Wide-Angle X-ray Scattering (GIWAXS), as well as by density functional theory (DFT) calculations and molecular dynamics (MD) simulations.

2. Results and discussion

The synthesis of the polymers is shown in the supporting information (SI). Since increasing molecular weight generally reduces the solubility of the polymers [57], especially for the random copolymers, the modest molecular weight was fixed to ensure sufficient solubility and thus processability. To exclude influence from molecular weight (Mn) and polydispersity (Đ = Mw/Mn), the four polymers were synthesized to have nearly identical Mn and Đ (Table 1, and **SI**). Moreover, CV measurements showed that all the polymers have comparable ionization energy (IE) values, all ranging between −4.9 eV and −5.0 eV (Table 1, and **SI**). Note that several recent reports used random copolymerization as an effective strategy to improve the HOMO level of the reference polymers, leading to higher doping efficiency [58–60]. In contrast to the aforementioned systems, here we do not alter the HOMO level of our polymers. Thus, we can also exclude that the difference in their electrical performance is caused by their different energy levels. Differential scanning calorimetric (DSC) measurements of P[$(3HT)_{1-x}$-stat-$(T)_x$] showed that both the crystallinity and melting temperature gradually decreased from P3HT to P[$(3HT)_{0.88}$-stat-$(T)_{0.12}$], P[$(3HT)_{0.76}$-stat-$(T)_{0.24}$] and P[$(3HT)_{0.64}$-stat-$(T)_{0.36}$], respectively (**SI**).

IEss: ionization energy in solid state; EAss: electron affinity in solid state. Tg: glass transition temperature of neat polymers from the peak loss modulus in dynamic mechanical analysis (DMA) first heating thermograms recorded at 1 Hz.

2.1. Electrical measurements and doping characterizations

To assess the electrical properties of these polymer semiconductors, OFET devices were fabricated in bottom-gate bottom-

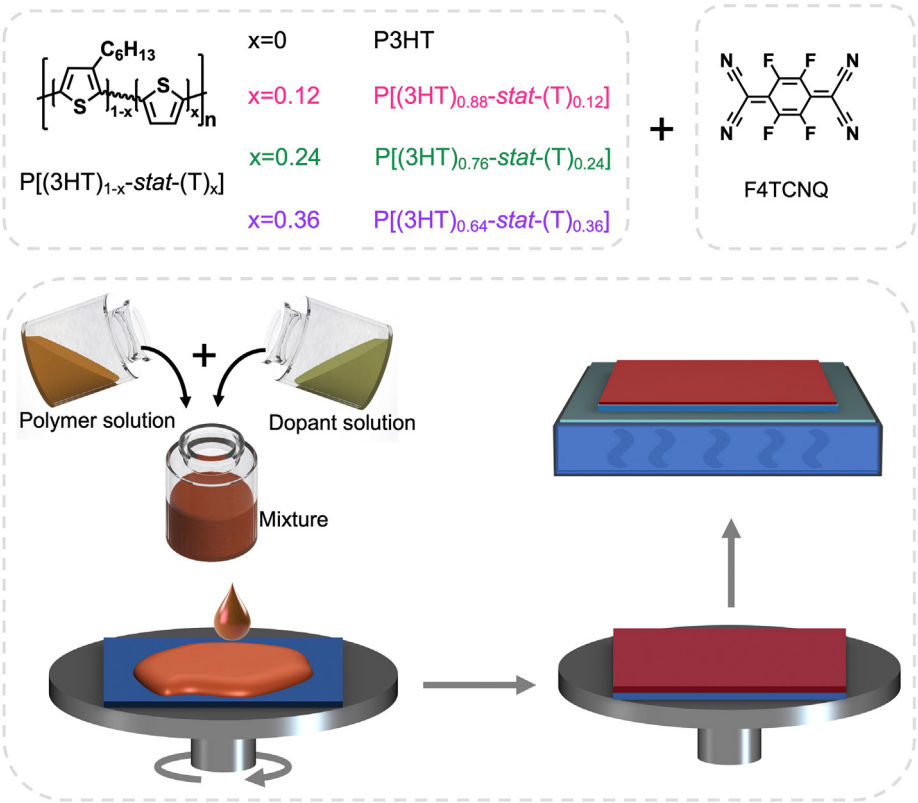

Fig. 1. Molecular structures of the polymers and dopant, as well as an illustration of mix-solution doping method.

Table 1
Summary of P[(3HT)$_{1-x}$-stat-(T)$_x$] information.

x value	Mn (kg/mol)	Đ	Tg(°C)	EgOpt (eV)	IESS (eV)	EASS (eV)
0	16.8	1.63	11	1.92	−4.94	−3.03
0.12	16.8	1.62	32	1.93	−4.97	−3.04
0.24	16.7	1.67	34	1.95	−4.91	−2.95
0.36	17.1	1.65	56	1.96	−5.00	−3.04

contact architecture and the charge carrier mobility (μ) for these pristine polymers was determined to be comparable (Fig. 2**A**, **2B**). Then, the polymers were doped by F4TCNQ using a mixed-solution doping method. Fig. 2**C** shows the evolution of the electrical conductivity of the polymer films as a function of the F4TCNQ molar ratio. P3HT exhibited a conductivity of 6.6 (±0.5) × 10^{-5} S cm^{-1} at 0.2 mol% F4TCNQ concentration, and dramatically reached its maximum conductivity of 1.9 (±0.2) × 10^{-2} S cm^{-1} at an F4TCNQ concentration of 2.5 mol%. This value is very comparable to the previous reports on the doped P3HT, for instance the one by Kim et al. [23] and the other by Hu et al. [26], though, it is lower than that of the state-of-the-art doped P3HT due primarily to the lower Mn in the current study. It was shown that increasing the Mn by ca. 5 times led to an increase in conductivity by ca. 1 order of magnitude [61]. The reported high-performing mixed-solution-doped P3HT usually has much higher Mn, for instance at the level of 60 KDa [62]. At doping ratios higher than 2.5 mol%, the conductivity of doped P3HT began to monotonically decline (Fig. 2C), resembling that of the previous report [26].

By comparison, P[(3HT)$_{0.88}$-stat-(T)$_{0.12}$] exhibited a conductivity of 1.4 (±0.3) × 10^{-5} S cm^{-1} at 0.2 mol% F4TCNQ concentration, and reached its maximum conductivity of 0.11 ± 0.04 S cm^{-1}, about 5 × larger than that of P3HT. Moreover, the maximum conductivity was reached at 10 mol% F4TCNQ concentration, suggesting a higher tolerance to dopant-induced disorder. Remarkably, P[(3HT)$_{0.76}$-stat-(T)$_{0.24}$] and P[(3HT)$_{0.64}$-stat-(T)$_{0.36}$] can be doped to significantly higher maximum conductivity of 2.1 (±0.14) S cm^{-1}, and 2.4 (±0.23) S cm^{-1}, respectively, over 2 orders of magnitude larger than that of P3HT. To the best of our knowledge, these values are among the best ever reported for F4TCNQ-doped P3HT by mixed-solution method [23–25,35,62].

To evaluate the activation energy (EA) of the doped polymer films, variable-temperature conductivity measurements were performed on the 10 mol% F4TCNQ doped polymers. As shown in Fig. 2**D**, the EA is determined to be 143.1, 119.5, 48.1, and 31.6 meV for P3HT, P[(3HT)$_{0.88}$-stat-(T)$_{0.12}$], P[(3HT)$_{0.76}$-stat-(T)$_{0.24}$] and P[(3HT)$_{0.64}$-stat-(T)$_{0.36}$], respectively, indicating increased hole-transport efficiency in the same order. The gradually decreased E_A suggests that a lower degree of charge traps or energetic disorder in the doped films is achieved with increasing T content. Furthermore, we performed ESR measurements to investigate the polaron feature of the doped polymers. As shown in Fig. 2**E**, apparent ESR peaks could be observed for all four doped polymers at a doping ratio of 10 mol%, suggesting the polaron formation after doping [14,38]. However, it is noted that a decrease in the peak intensity was observed as the T content increased, even when the semiconductor and dopant amounts were kept the same. The spin numbers of the doped samples were obtained by comparing their second integral of ESR signals with that of the standard sample, according to the equation and method reported by Neher et al. [63] Consequently, the double integration of the ESR signal which reflects the spin density in the doped films follows the trend of P3HT > P[(3HT)$_{0.88}$-stat-(T)$_{0.12}$] > P[(3HT)$_{0.76}$-stat-(T)$_{0.24}$] > P[(3HT)$_{0.64}$-stat-(T)$_{0.36}$] (Fig. 2**F**), for instance, with a spin density of 2.83 × 10^{22}, 2.54 × 10^{22}, 2.40 × 10^{22}, and 2.20 × 10^{22} mol^{-1} being

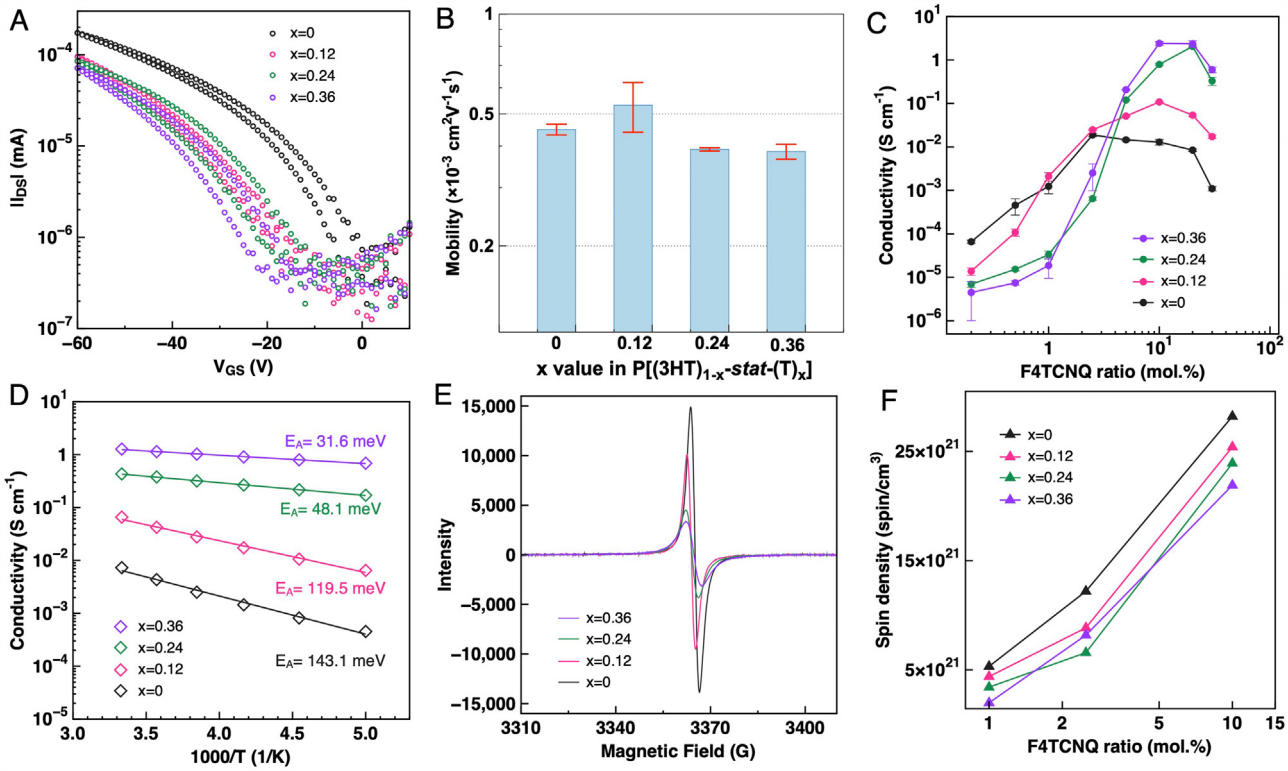

Fig. 2. (A) Transfer curves and (B) charge carrier mobility of pristine films of P[(3HT)$_{1-x}$-stat-(T)$_x$], (C) electrical conductivity of doped polymer films as a function of dopant concentration. (D) temperature dependence of the electrical conductivity and (E) ESR results for 10 mol% doped polymer films, and (F) The spin density in the doped films extracted by double integration of the ESR signal.

determined at 10 mol%, respectively, suggesting that the number of polarons is decreased as the T content increases.

2.2. Microstructure and molecular packing

GIWAXS was performed to further investigate the effect of doping on the microstructure evolution of all the polymer films. As shown in the 2D diffraction patterns in Fig. 3**A** (top row), all polymers exhibit lamellar packing with predominant edge-on orientations of the polymer backbone. More specifically, as indicated by the GIWAXS pattern of P3HT film, both well-ordered out-of-plane peaks (h00) and in-plane π stacking peaks can be clearly seen, indicating pronounced long-range crystallinity. However, the GIWAXS pattern for P[(3HT)$_{1-x}$-stat-(T)$_x$] is diffuse as compared to that of P3HT, implying a less pronounced long-range order for the random copolymers. It is worth mentioning that the pristine P(3HT)$_{0.64}$-(T)$_{0.36}$ film exhibits random orientation as indicated by the full ring of scattering in the GIWAXS pattern. The GIWAXS results are in agreement with the DSC measurements that the crystallinity decreased with the increasing amount of T. Note that for all films, a diffuse arch of scattering at a radial q ~1.65 Å^{-1} is assigned to isotropic side-chain packing. After doping at an F4TCNQ concentration of 10 mol%, as shown in Fig. 3**A** (bottom row), the crystallinity of doped P3HT film decreases in comparison to pristine P3HT film, as indicated by the diminishing out-of-plane peaks and the more diffuse ring, By contrast, a drastic increase in long-range order is observed for the T containing P[(3HT)$_{0.88}$-stat-(T)$_{0.12}$], P[(3HT)$_{0.76}$-stat-(T)$_{0.24}$] and P[(3HT)$_{0.64}$-stat-(T)$_{0.36}$]. Furthermore, these doped P[(3HT)$_{1-x}$-stat-(T)$_x$] films adopt a substantially more ordered structure, as indicated by the strong 2nd- and 3rd-order lamellar peaks, and the pronounced π-π stacking peak.

Vertical line integrations along q_z were made to evaluate the lamellar stacks corresponding to edge-on polymers. As shown in Fig. 3**B** (left), in the pristine films, the lamellar stack is shortened with the increasing content of T until it reaches a threshold value of 36%, where the pristine P[(3HT)$_{0.64}$-stat-(T)$_{0.36}$] film has only an insignificant amount of edge-on packing backbones. As shown in Fig. 3**B** (right), in the doped films, the lamellar packing distance keeps shrinking as more T is introduced in the polymers. Remarkably, a drastic increase in the overall crystallinity is seen in the doped system with more T introduced in the polymers, with a maximum crystallinity reached for x = 0.24. Hereby, the most intense (100) peak in the case of the 24% T-containing system indicated a most pronounced crystallinity of the doped P[(3HT)$_{0.64}$-stat-(T)$_{0.36}$] film.

To evaluate the π-π stacking and side-chain packing of the polymer films, horizontal line integrations along qxy were also made. As shown in Fig. 3**C** and Fig. S7A, in the pristine films of P(3HT)$_{1-x}$-(T)$_x$, the overall scatting intensity is relatively low. By contrast, in the doped P(3HT)$_{1-x}$-(T)$_x$ system, it is evident that the overall scattering intensities are substantially higher than that of their pristine counterparts. Moreover, the doped films possess actual π-π stacking which becomes shorter as more T is introduced. This explains well the much higher electrical conductivity observed in the case of doped P[(3HT)$_{0.76}$-stat-(T)$_{0.24}$] and P[(3HT)$_{0.64}$-stat-(T)$_{0.36}$]. All fitted values of the lamellar and π-π stacking distances are shown in Table 2. Remarkably, both doped P[(3HT)$_{0.76}$-stat-(T)$_{0.24}$] and P[(3HT)$_{0.64}$-stat-(T)$_{0.36}$] display an additional peak at

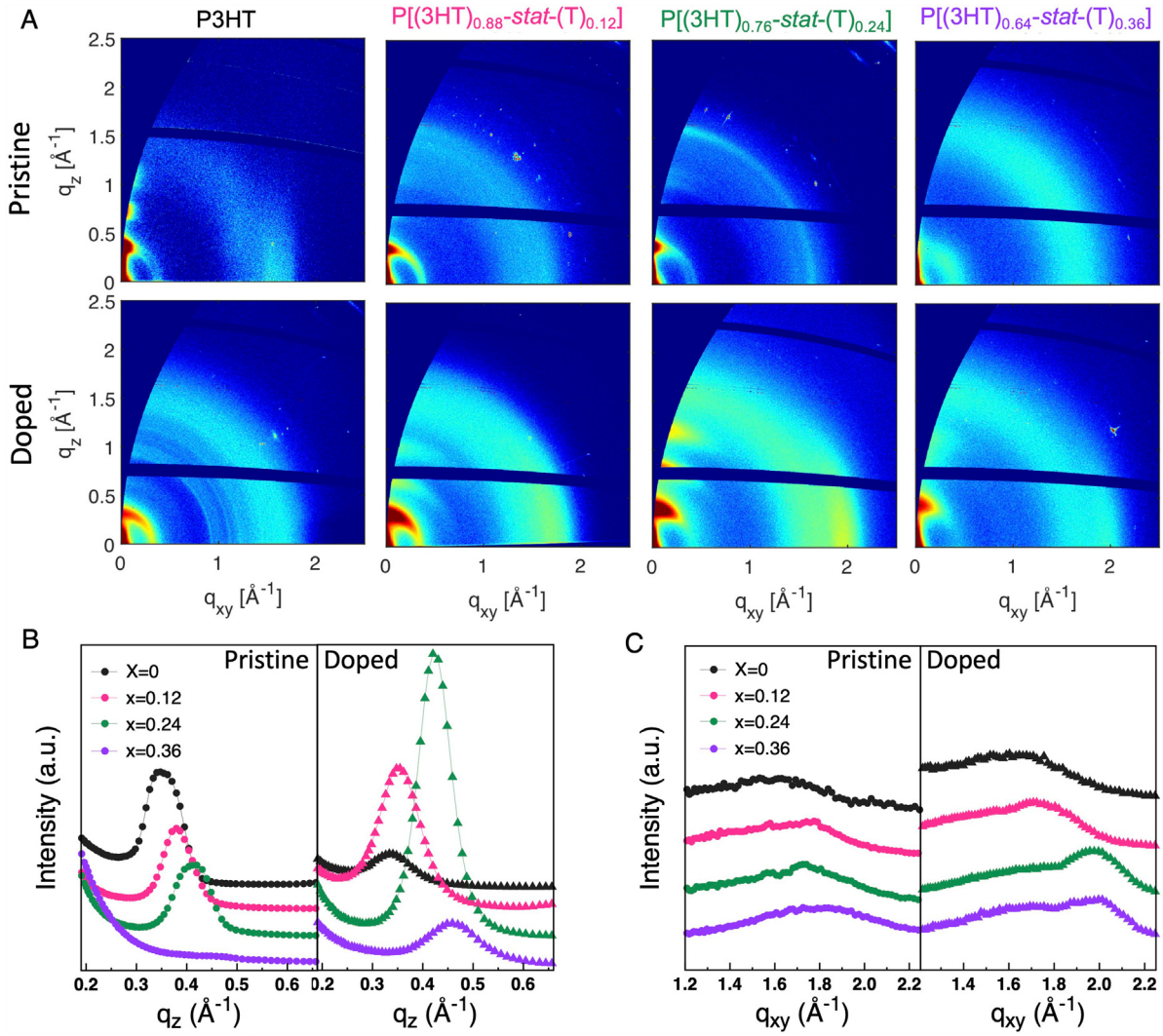

Fig. 3. (A) 2D GIWAXS patterns of pristine (top row) and 10 mol% doped (bottom row) polymer thin films. (B)Vertical line integration around the lamellar peak in q_z for the pristine and doped polymers. (C) Horizontal line integration around the π-π peaks in q_{xy} for the pristine and doped polymers.

Table 2
GIWAXS quantitative data of pristine and doped P[(3HT)$_{1-x}$-stat-(T)$_x$].

x value	P/D[a]	Lamellar (100)		π-π (010)	
		d[b]-(Å)	CL[c] (nm)	d-(Å)	CL (nm)
0	P	16.99	66.0	3.63	–
	D	18.48	52.4	–	–
0.12	P	16.43	71.0	–	–
	D	17.73	55.8	3.53	16.2
0.24	P	15.27	62.4	–	–
	D	14.81	59.5	3.15	21.6
0.36	P	–	–	–	–
	D	13.64	40.9	3.13	21.4

A P/D represents Pristine/Doped. b d means d-spacing, CL means coherent length.

~2.01 Å^{-1} corresponding to a much tighter packing distance of 3.15 Å and 3.13 Å. With the help of DFT calculations, we infer that such a short stacking distance comes from the packing between polymer and dopant molecules and more details are shown in section 2.4.

Atomic force microscopy (AFM) was performed on the pristine and doped polymer films (Fig. 4). No distinct differences could be observed in the AFM image of the pristine P3HT and P[(3HT)$_{0.76}$-stat-(T)$_{0.24}$] films, as shown in Fig. 4**A** and **B**. However, after doping, the morphology of P3HT is disrupted and the film surface becomes much rougher (Fig. 4**C**), which is consistent with the GIWAXS measurement. By contrast, fibrous structures could be identified in the AFM image of doped P[(3HT)$_{0.76}$-stat-(T)$_{0.24}$] film (Fig. 4**D**) indicating a higher long-range order, again in agreement with the GIWAXS measurement as shown in Fig. 3 and Table 2.

2.3. Optical absorption spectroscopy

To further understand the effect of T content, UV–vis–NIR absorption was performed on both pristine and 10 mol% doped films of all four polymers. As shown in Fig. 5**A**, the spectrum of pristine P3HT films shows a main band at around 550 nm, a typical feature resembling previously reported spectra in the literature [62,64]. After doping, two new strong and broad bands appear at around 770 nm and 860 nm (Fig. 5**A**) corresponding to local excitations in the anionic F4TCNQ species (F4TCNQ^{-1}), and the polaron band was also nicely reproduced by the modeling as shown in Fig. 5**G** and in agreement with previous reports [62,64]. Similarly, as shown in Fig. 5**B**, **C**, and **5D**, the pristine films P[(3HT)$_{0.88}$-stat-(T)$_{0.12}$], P[(3HT)$_{0.76}$-stat-(T)$_{0.24}$] and P[(3HT)$_{0.64}$-stat-(T)$_{0.36}$] all exhibits

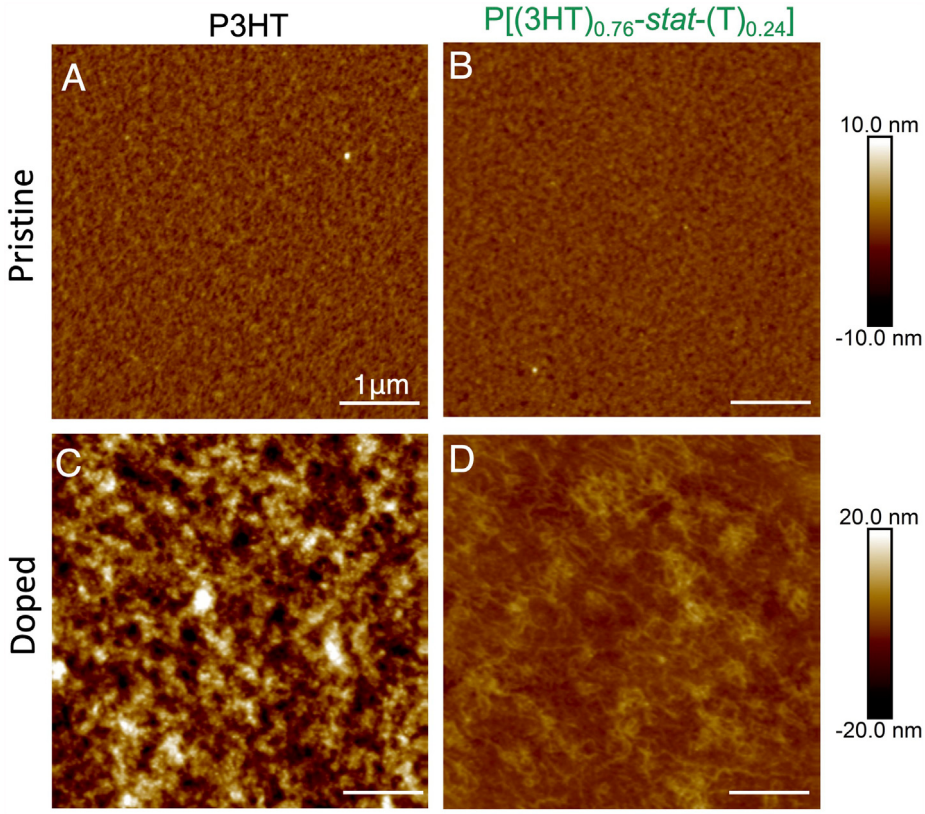

Fig. 4. AFM images of the pristine (top row) and doped (bottom row) P3HT and P[(3HT)$_{0.76}$-stat-(T)$_{0.24}$] films.

almost identical features as P3HT films. As shown in Fig. 5**E**, while the direct comparison in this respect between P[(3HT)$_{0.76}$-stat-(T)$_{0.24}$] and P3HT may be blurred because of structural differences, the pronounced vibrational progression in the case of P[(3HT)$_{0.76}$-stat-(T)$_{0.24}$] indicates a non-negligible level of intermolecular aggregation [65]. In Fig. 5**F**, it is shown that the relative intensity of the bands at 770–860 nm and 2000–2400 nm decreases with increasing T content, indicating the decreased density of both F4TCNQ^{-1} and the polaron T7^{+1}. More discussions will be presented in section 2.5. The optical spectra are consistent with the ESR data that the polarons density becomes lower with the increase of T content.

2.4. Computational study

In order to elucidate the origin of these facts, first we focus on the origin of the short-contact of 3.15 and 3.13 Å. To this aim we simulated several π-π stacked model-polymer dimers as shown in Fig. 6. The geometries of these complexes were optimized in the frame of DFT theory by employing the ωB97XD functional and the 6-31G(d,p) basis set. In order to mimic the strongest interaction between two polymer chains, we optimized the geometries of cofacially stacked dimers made up of model-polymer backbones containing 15 repeat units, with side chains (TCH3 in our simulations) or without side chains (T), see Fig. 6**A** and **B**. Model copolymers containing 33% bare T units combined with T-CH3 units in two different ways were also calculated (Fig. 6**C** and **D**). In all cases, standard π-π stacking distances ranging from 3.64–3.72 A° were observed, which are much larger than the experimental distance of 3.13 A°.

Given that these cofacial-like π-stacking interactions are the strongest that can be established between π-conjugated backbones, we are consequently left with the conclusion that the dopant is necessarily involved in these very-short contacts (dopant-polymer complex). Herein, we use one model polymer containing seven thiophene rings (named as T7) and another model polymer containing 10 thiophene rings (named as T10), thus a complex between the polymer TCNQ being T7—F4TCNQ and a complex constructed with F4TCNQ and two model polymers being T10—F4TCNQ—T10. Accordingly, here we first consider isolated T7—F4TCNQ and T10—F4TCNQ—T10 model complexes mutually oriented in a π-π stacked manner (Fig. 7**A** and **B**). The result indicates average F4TCNQ—T7 and F4TCNQ—T10 distances of only 3.23 Å and 3.25 Å, respectively, in good agreement with the experimentally observed value of 3.13 Å. In order to consider the impact of the side chains in the positioning of the F4TCNQ in between the two polymer chains, fourteen-ring chains were considered, each chain containing three consecutive bare thiophenes and eleven rings substituted with hexyl side chains. The calculations for this system were carried out in the frame of the extended tight binding method [66] and resulted in average F4TCNQ—polymer distances of 3.15 Å (Fig. 7**C** and **D**), in excellent agreement with the experimental value of 3.15 and 3.13 Å.

In order to obtain a statistical view on the intermolecular distances in the systems under study, MD simulations were carried out on mixtures of ten-ring bare polythiophene (PTT), ten-ring polythiophene derivatives containing three bare thiophene rings and seven rings containing hexyl substituents (P3TT, representative of P[(3HT)$_{0.76}$-stat-(T)$_{0.24}$] and P[(3HT)$_{0.64}$-stat-(T)$_{0.36}$]), and P3HT model polymers with F4TCNQ (Fig. S8). Hereby, the 10 mol% doped P3TT model polymers correspond to one F4TCNQ molecule per 10 thiophene rings. In each case, the simulation box contains 392 monocationic model polymers of ten thiophene rings (P3TT and P3HT) and 392 monoanionic F4TCNQ molecules. For the bare PTT,

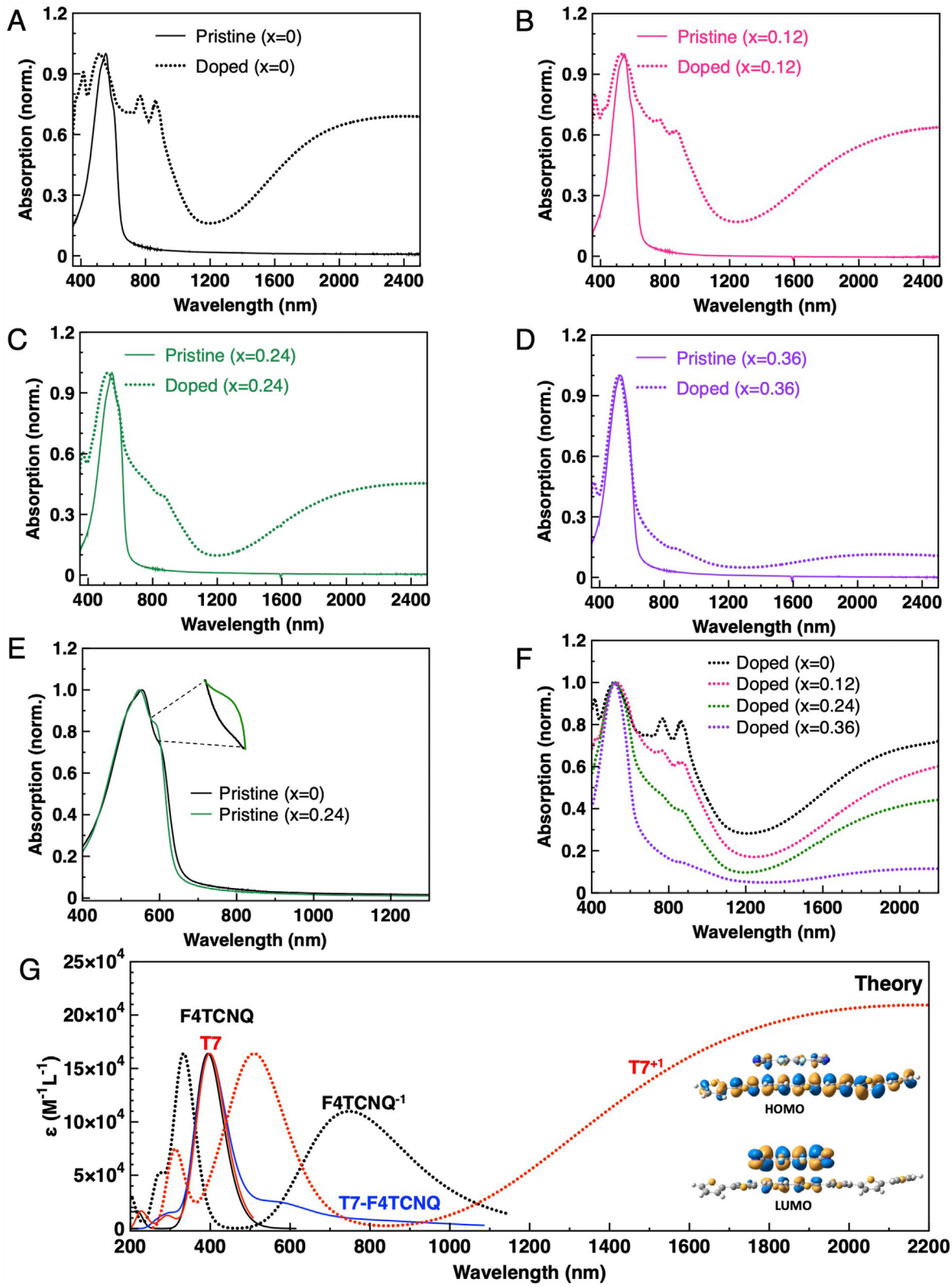

Fig. 5. Normalized UV–vis–NIR absorption spectra for thin films of pristine and 10 mol% doped (A) P3HT, (B) P[(3HT)$_{0.88}$-stat-(T)$_{0.12}$], (C) P[(3HT)$_{0.76}$-stat-(T)$_{0.24}$], and (D) P[(3HT)$_{0.64}$-stat-(T)$_{0.36}$]. (E) comparison between pristine P3HT and P[(3HT)$_{0.76}$-stat-(T)$_{0.24}$], (F) comparison between doped P3HT and P[(3HT)$_{1-x}$-stat-(T)$_x$]. (G) theoretical absorption spectra of different species calculated by means of time-dependent (TD) DFT method at the ωB97XD/6-31G(d,p) level (inserted images are HOMO and LUMO of the model F4TCNQ—P3TT co-crystals).

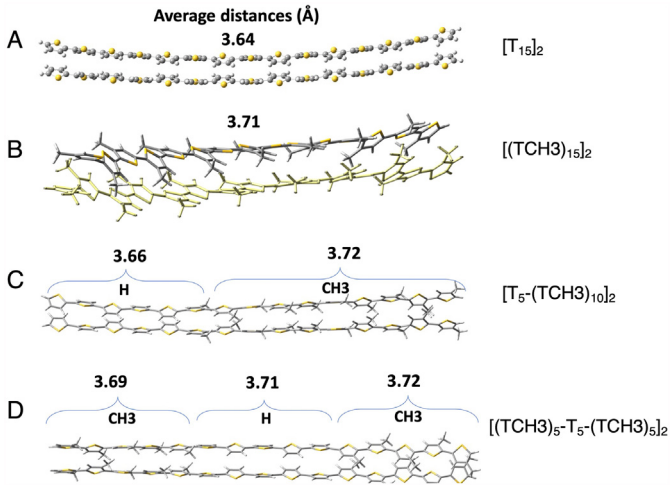

Fig. 6. Theoretical geometries of dimers constructed by considering two π-π stacked polymer-chain models, each of them containing 15 thiophene rings. Each chain contains, from top to bottom: bare thiophenes [T15]2, methyl-substituted thiophenes [(TCH3)15]2, [T5-(CH3)10]2, and [(CH3)5-T5-(CH3)5]2, respectively. The distances in angstroms correspond to the average distance between each Carbon- or Sulphur atom of one chain with the nearest C- or S atoms of the other chain. Note that this distance may be slightly larger than the average distance between the mean-planes of the two chains (π-π stacking distance). In the case of chains containing a mixture of T and T-CH3 rings, the distances for each fragment are indicated. All results were obtained at the ωB97XD/6-31G(d) computation level.

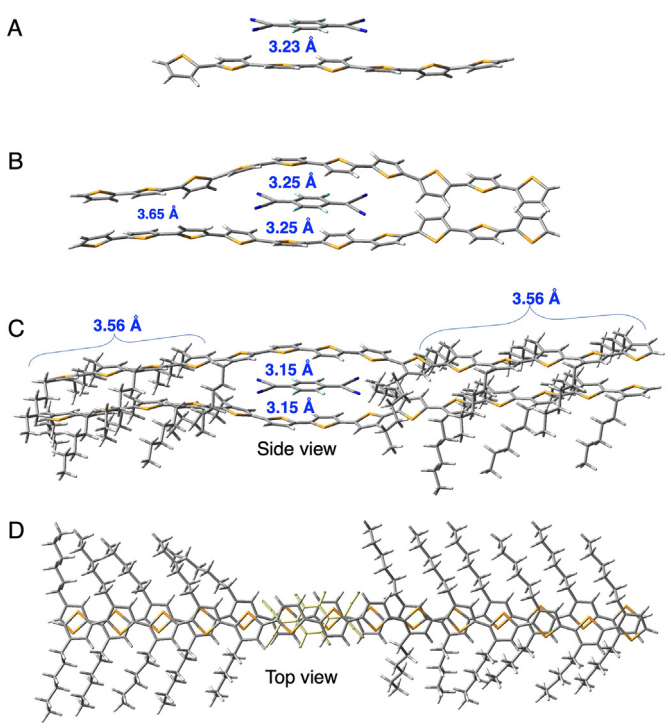

Fig. 7. (A) Theoretical geometry of a dimer constructed with F4TCNQ and one model donor-polymer containing seven thiophene rings. The shortest distances (average) between the donor chain and F4TCNQ is 3.23 Å. (B) Theoretical geometry of a complex constructed with F4TCNQ and two model donor-polymers, with the former intercalated in between the two later ones. Each model donor-polymer is constituted by 10 thiophene rings. The shortest distances (average) between the two donor chains and between each of them and the F4TCNQ molecules are 3.25 Å. All results were obtained at the ωB97XD/6-31G(d) computation level. (C) (D) Complex containing F4TCNQ sandwiched in between two 14-ring model polymers, each model polymer containing three bare thiophenes and 11 rings substituted with hexyl chains. The calculations were based on the extended tight binding method as implemented in the xTB software.

707 monocationic model polymers with an equal number of monoanionic F4TCNQ were inserted. The distributions of the dopant-polymer distances along with their π-π orientations are shown in Fig. 8**A**–**C**. The aromatic ring of F4TCNQ tended to tilt at a small angle with respect to the nearest thiophene ring, with 0° corresponding to a planar orientation. For P3HT- F4TCNQ, it peaked at 0.35 nm at 25°, whereas for P3TT- F4TCNQ and PTT-F4TCNQ it peaked at 0.35 nm at 23° and 0.33 nm at 20° respectively, with a few examples of extracted orientations shown in Fig. S9. Such titled orientations are the result of numerous C—H···F, and C—H···N interactions, despite their weak strength. Since P3HT has more such interactions as a result of the presence of more hexyl substituents, the titled angle for F4TCNQ-P3HT is thus larger. The distributions of the dopant-polymer distances are shown in Fig. 8**D**–**F** with maximum probabilities corresponding to distances of 0.34–0.36 nm, 0.32–0.34 nm, and 0.31–0.33 nm for P3HT, P3TT, and PTT, respectively, demonstrating a reasonable agreement with the experimental value of 3.13 Å for doped P3TT. The average polymer-polymer distances follow the trend 0.34 nm < 0.39 nm < 0.40 nm respectively for PTT, P3TT, and P3HT, in line with the increasing number of hexyl substituents in the chains (Fig. S10).

We also calculated the 2-D wide-angle X-ray scattering structure factor for the simulated film [68], as shown in Fig. S7B. The q_z and q_{xy} parameters were obtained by summing the axial components. Interestingly, the peaks correspond to the major features of the GIWAXS as shown in Fig. 3. It is worth noting that in the simulated wide-angle X-ray scattering, the details such as the experimental peak ~2 $Å^{-1}$ are (i) overwhelmed by diffuse signals coming from isotropic side-chain packing, and (ii) are most noticeable in P3TT-dopant system. Hereby, the less distinct peak at ~2 $Å^{-1}$ is conditioned by the high computational resources required to scale beyond 1000 nm^3 box size. We can see that the 1.53 $Å^{-1}$ peak in P3TT-dopant corresponds closely to P[$(3HT)_{0.64}$-stat-$(T)_{0.36}$]), which is the isotropic side chain packing. The peak at ~1.5 $Å^{-1}$ corresponds to the maximum probability of distance between two separate polymers as shown in Fig. S10. The overall shape of the simulated diffraction correlated with the polymer-polymer distance distribution is also clearly seen in the P3TT diffraction pattern and P3TT-P3TT distance distribution. However, the small peak at ~2 $Å^{-1}$ in the P3TT-dopant system corresponds to the maximum probability for the P3TT-dopant distance as shown in Fig. 8E.

Taken together, the DFT, xTB, and MD simulations in concert support the short π-π stacking distance of 3.13 Å stemming from the π-stacking intercalation of the dopant molecules in-between the polymer chains. These results can be well explained by the facts that (i) the F4TCNQ molecule is perfectly flat, and (ii) the polymer-F4TCNQ (donor-acceptor) interactions are stronger than standard π-π stacking interactions due to the additional hole-electron coulomb attractive interactions.

The images shown in Fig. S11 are the 3-D discrete Fourier transform of F4TCNQ in P3HT, P3TT, and PTT. The distance between two sharp lines corresponds to twice the spatial frequency of intermolecular distance between the two F4TCNQ molecules. The sharpness of the lines is an indication of the degree of F4TCNQ order inside the polymers. A plot of the probability distribution of the intermolecular distance between dopants yielded a mean distance of 0.99(±0.23) nm, 0.74(±0.18) nm, and 0.97(±0.26) nm for P3HT, P3TT, and PTT respectively (Fig. S12). To take a closer view, the corresponding 2-D images of the 3-D discrete Fourier transform are shown in Fig. 8**G**–**I**. As it can be clearly seen, the lines are sharper and better defined in P3TT (Fig. 8**H**) than that in P3HT (Fig. 8**G**) and PTT (Fig. 8**I**), indicating F4TCNQ is better ordered in

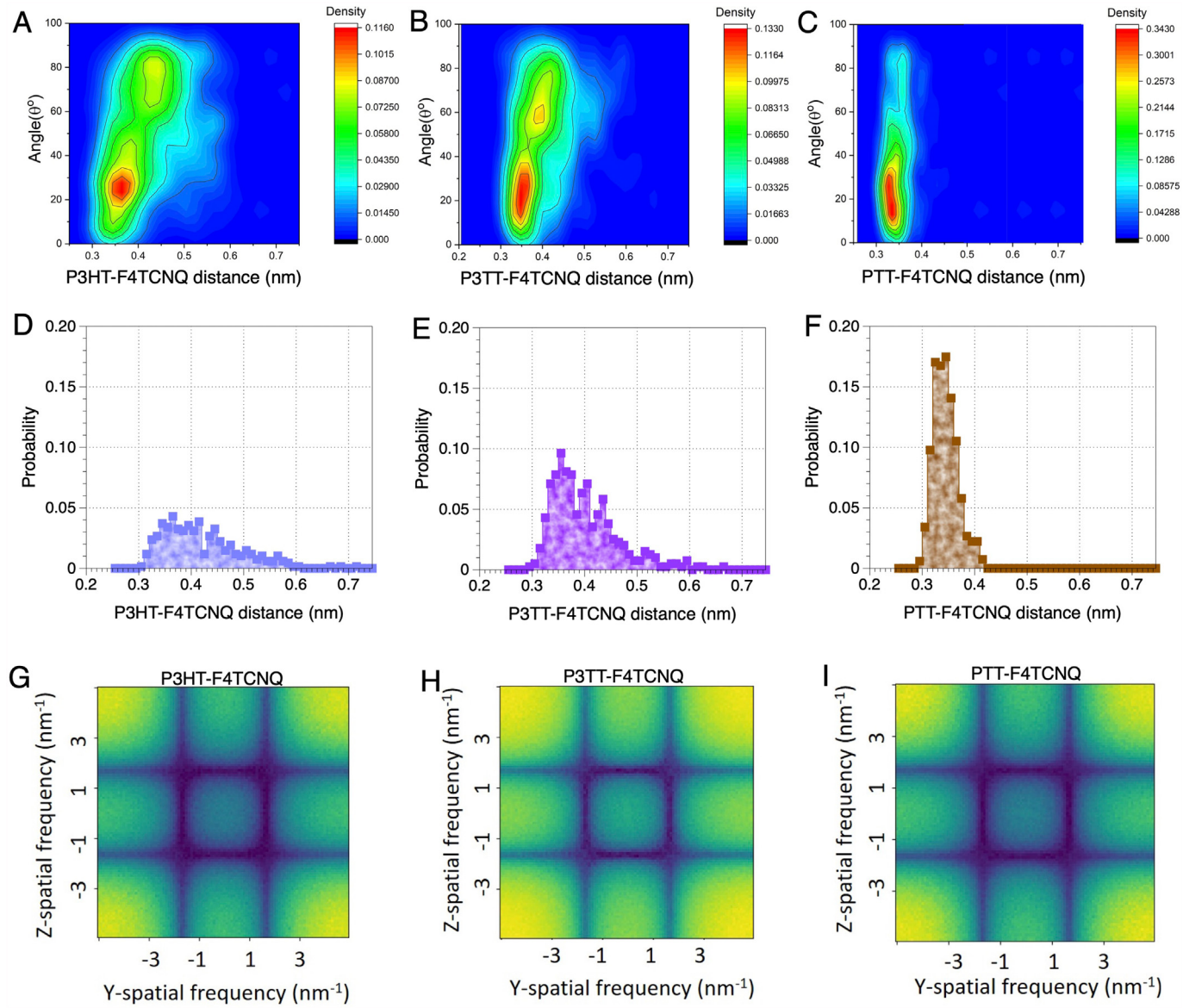

Fig. 8. Results from molecular dynamics simulations on mixtures of P3HT, P3TT, and PTT model polymers with 10% mol of F4TCNQ. Probability density distribution of distance versus orientation of F4TCNQ with respect to polymer (A) P3HT- F4TCNQ, (B) P3TT-F4TCNQ and (C) PTT-F4TCNQ. The probability distribution of distance between (D) P3HT-F4TCNQ, (E) P3TT-F4TCNQ and (F) PTT-F4TCNQ. The 2-D images of 3-D discrete Fourier transform viewed from side-chain interdigitation for F4TCNQ in (G)P3HT, (H)P3TT, and (I)PTT.

P3TT. Similar information can be observed in the MD simulation Figures shown in Fig. S13.

2.5. Discussion

The theoretical results discussed in the previous section suggest that the dopant molecules in these systems are playing a double role, in addition- or instead to the classical doping one: (i) a "bridging" role between two π-π stacked polymer chains, given that the polymer-bridge distances are smaller than the polymer-polymer ones. (ii) a "gluing" role by establishing two short-distance strong interactions with two polymer chains. Each dopant molecule reduces the freedom degree in the interchain oscillations that the two polymers would have in the absence of bridging, thus contributing to locally increasing the short-range order. The importance of the bridging-gluing effect is discussed below.

2.5.1. *Impact of polymer-dopant-polymer supramolecular system on the doping level*

We now shift our attention to the decrease of the polaron density with the increasing T content in the copolymers. This conclusion was deduced from both the ESR and optical absorption spectra. From the optical experimental observations, the relative intensity of the bands at 770–860 nm and 2000–2400 nm corresponding to $F4TCNQ^{-1}$ and the $P3HT^{+1}$ decreases with increasing T-content from P3HT to $P[(3HT)_{0.64}\text{-stat-}(T)_{0.36}]$. The decrease in relative intensity of the 770–860 nm band can be easily explained by the decreased concentration of the $F4TCNQ^{-1}$ species in the films, given that the F4TCNQ molecules become more and more involved in π-π interactions with the polymer chains of increasing T-content, as supported by both GIWAXS and modeling results. These conclusions are also supported by the comparison between the theoretical optical spectra of the model π-stacking complex T7-F4TCNQ, and the charged dopant- and model-polymer shown in

Fig. 5G: both polaronic bands characteristics of $F4TCNQ^{-1}$ and $T7^{+1}$ are absent in the spectrum of T7-F4TCNQ, suggesting for F4TCNQ in the π-stacking complex a different role as compared to its conventional doping function. Indeed, as suggested by the mixing between the dopant and polymer frontier orbitals (Fig. 5G, inserted figures), only a partial charge transfer can occur between the π-π stacked F4TCNQ—P3TT structure. Specifically, in the case of the complex 4FTCNQ—T7, only a portion of 0.2e charge transfer is found by our DFT calculations, which is in very good agreement with the theoretical (0.24e) and experimental (0.21e) charge transferred values determined for terthiophene T4-F4TCNQ [64]. Interestingly, such a co-crystal has been suggested by Salzmann et al. to act as a new quasi-dopant undergoing electron transfer with an adjacent neat polymer segment resulting in a couple of $F4TCNQ^{-1}$ and positively charged polymer [64].

Based on the fact that the vibration frequencies of the CN bonds are different in F4TCNQ pristine films, in the polythiophene films acting as dopants, and in the polymer-dopant charge-transfer complex (bridging-gluing), we have performed theoretical calculations on IR spectra and FTIR measurement (Fig. S14). Our calculations predicted a negative shift of roughly 50 cm^{-1} for $F4TCNQ^{-1}$ as compared to the neutral one, and only 7 cm^{-1} for the CT complex T7-F4TCNQ. Interestingly, though, the FTIR spectra (Fig. S14) only detect the presence of anionic F4TCNQ, which signal is blue-shifted by some 45 cm^{-1} as compared to the signal of the neutral F4TCNQ. The FTIR results consequently allow for excluding the presence of partial charge transfer in the doped copolymers, which seems coherent with the suggestion from Salzmann et al. about the presence of dopant-copolymer complexes as a new doping unity [64]. Moreover, the presence of neutral F4TCNQ in the doped mixture cannot be detected, given that the FTIR signal corresponding to neutral F4TCNQ has a much lower extinction coefficient than its anion, and hence the signal is usually too weak to be seen [67].

All in all, the results from GIWAXS, DFT, the FTIR, and from the literature directly or indirectly confirm that part of the F4TCNQ dopant molecules do intercalate in a π-stacked manner in-between two adjacent copolymer chains at the regions of pure-T occurrence. Donor-Acceptor π-conjugated complex is thus created, adopting two possible situations: (i) F4TCNQ remains neutral in the π-conjugated complex due to inappropriate geometrical- or polarization environments. These molecules can be considered as "lost" dopants for the doping role, thus explaining the decrease in the polaron density. This is statistically favoured at a very low doping level, which is in agreement with the experimental results (Fig. 2F). (ii) The π-conjugated complex acts as a new quasi-dopant undergoing electron transfer with an adjacent neat polymer segment resulting in a couple of $F4TCNQ^{-1}$ and positively charged polymer [64]. We speculate that due to the strong interactions between the bridged F4TCNQ and the copolymers chains, the two separated electrons (one in the dopant and one on the copolymer) remain coupled close to each other and become ESR-silent, which is not the case for the normal doping of P3HT.

The trend in the charge density at 10 mol % of F4TCNQ is corroborated with the number N of consecutive T rings in the polymer chains, with N roughly being 0, 1–2, 2–3, and 3–4 for P3HT, $P[(3HT)_{0.88}\text{-stat-}(T)_{0.12}]$, $P[(3HT)_{0.76}\text{-stat-}(T)_{0.24}]$ and $P[(3HT)_{0.64}\text{-stat-}(T)_{0.36}]$, respectively. Fig. 8**A**–**D** clearly shows that the size of F4TCNQ along the long-axes direction is roughly equal to the length of three consecutive T rings. Accordingly, two- or fewer consecutive T rings offer less room for the establishment of short-distance π-π stacking and strong π-π interactions, due to the presence of side chains and larger inter-ring dihedral angles. This simple comparison suggests that the shortest distance and the strongest interaction between the dopant and the chain can occur in the case of $P[(3HT)_{0.76}\text{-stat-}(T)_{0.24}]$ and $P[(3HT)_{0.64}\text{-stat-}(T)_{0.36}]$, thus providing a qualitative explanation for their similarly larger hole conductivities. Thus, the polymer-dopant-polymer sandwich supramolecular system resulted in a smaller amount of charges in the doped random polymer.

2.5.2. *Impact of polymer-dopant-polymer supramolecular system on the charge transport*

The increased hole conductivity despite the decreased polaron density of the doped $P[(3HT)_{1-x}\text{-stat-}(T)_x]$ as compared to doped P3HT points to the increased hole-mobility in $P[(3HT)_{1-x}\text{-stat-}(T)_x]$. This can be correlated with the presence of the very short π-π stacking distance of 3.13–3.15 Å, which we assume operates by means of two mechanisms: bridging and gluing.

We first focus on the bridging effect of F4TCNQ sandwiched between two copolymer chains. As a means to give a feeling of how much the electronic couplings can change with the distance between the π-stacked molecules, we reconsider the model complex T10-F4TCNQ-T10 (Fig. 8**B**) and the corresponding dimer T10-T10. Our calculations indicate that the electronic couplings between HOMO(T10)-LUMO(F4TCNQ) and HOMO(T10)-HOMO(T10) are 421 meV and 95 meV, respectively. While the phase- (mis)matching between the overlapping orbitals plays an important role, these electronic couplings and overlaps along with their trend do correlate with the interplanar distances of 3.25 Å and 3.64 Å (Table 2) determined for T10-F4TCNQ-T10 and T10-T10, respectively. However, the real charge transfer between two polymer backbones (say polymer1 and polymer2) bridged by F4TCNQ molecules is expected to proceed via a superexchange mechanism in a single step, which is much faster than that between two non-bridged polymer backbones (Fig. 9). With increasing the number of such bridges, the hole-transport efficiency increases, well explaining the hole-mobility difference between the doped $P[(3HT)_{1-x}\text{-stat-}(T)_x]$ and P3HT.

Supporting the above analysis by means of direct Hall measurement is challenging, given that this method can be held reliable only when the mobility values are high enough, say at least approaching 1 $cm^2V^{-1}s^{-1}$. In order to circumvent this difficulty, we followed two approaches. First, we deduced approximate values of the mobilities. Starting from the equation $\sigma = ne\mu$, where e is the fundamental charge, and n is the charge density (1.42×10^{22},

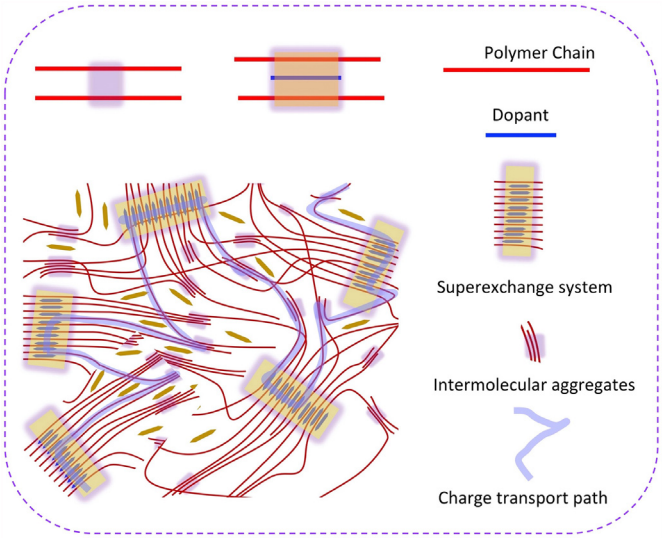

Fig. 9. Schematic illustration of the doped $P[(3HT)_{1-x}\text{-stat-}(T)_x]$ ($x \geq 0.24$) microstructure.

1.27×10^{22}, 1.20×10^{22}, and 1.10×10^{22} mol^{-1} for P3HT, P[(3HT)$_{0.88}$-stat-(T)$_{0.12}$], P[(3HT)$_{0.76}$-stat-(T)$_{0.24}$] and P[(3HT)$_{0.64}$-stat-(T)$_{0.36}$], respectively), which is half of the spin density as reported in Fig. 2**F**, we estimated the μ of 10 mol% doped films are 4.5 (±0.7) × 10^{-4} $cm^2V^{-1}s^{-1}$ for P3HT, 4.2 (±0.02) × 10^{-3} $cm^2V^{-1}s^{-1}$ for P[(3HT)$_{0.88}$-stat-(T)$_{0.12}$], 3.3 (±0.2) × 10^{-2} $cm^2V^{-1}s^{-1}$ for P[(3HT)$_{0.76}$-stat-(T)$_{0.24}$], and 1.1 (±0.1) × 10^{-1} $cm^2V^{-1}s^{-1}$ for and P[(3HT)$_{0.64}$-stat-(T)$_{0.36}$], respectively. Second, we performed TCNQ doping on the polymers instead of F4TCNQ to verify the effect of bridging-gluing. Hereby, TCNQ is structurally similar to F4TCNQ in both molecular size and shape, but has a quite different electron affinity value in solid state. Thus, it is expected that TCNQ should be able to intercalate between the random copolymer chains, creating a similar type of effect of bridging-gluing, though, it will not be able to dope the polymer due to the mismatching of the energy level between TCNQ and the P[(3HT)$_{1-x}$-stat-(T)$_x$]. Indeed, when doping P3HT and P[(3HT)$_{0.76}$-stat-(T)$_{0.24}$] with 10 mol% TCNQ, the charge transport is more efficient in the case of TCNQ-doped P[(3HT)$_{0.76}$-stat-(T)$_{0.24}$] than that in the TCNQ doped P3HT (Fig. S15).

Secondly, the gluing effect can also be correlated with the global increase in the long-range order of doped P[(3HT)$_{1-x}$-stat-(T)$_x$] as compared to their pristine films [58,69,70]. Hereby, the formation of polymer—dopant—polymer charge-transfer complexes reduces the random interchain positioning of polymers by keeping them tight, thus decreasing the positional disorder, and increasing chances for establishing along-chains π-π stacking overlaps and creating the potential for establishing stronger HOMO-HOMO interchain interactions. This is what is indeed observed experimentally, with the long-range order being drastically increased in the cases of P[(3HT)$_{1-x}$-stat-(T)$_x$] after doping (Fig. 3, Table 2). Such a PTT-F4TCNQ-PTT sandwich supramolecular system resembles the p-n co-crystals facilitating efficient charge-transport along the π-π stacking direction [71]. All in all, the bridging effect alone or gluing effect alone could explain the increase in the hole mobility thanks to the increase in the number of bridges and the increase in the long-range order, respectively. Favorably, these two effects are correlated and work in concert, with the common result being the increase in the hole mobility in the films of doped P[(3HT)$_{1-x}$-stat-(T)$_x$].

2.5.3. Impact of polymer-dopant-polymer supramolecular system on electrical conductivity

With the increasing concentration of F4TCNQ in the polymer films, two opposite effects can be observed: (i) increase of disorder due to the intercalation of F4TCNQ in-between the side-chains, causing a detrimental impact on the hole mobility, and (ii) increase of the bridging-gluing efficiency in P[(3HT)$_{1-x}$-stat-(T)$_x$] films, yielding beneficial impact on the hole mobility. While the disorder effect is almost the only one operating in the case of P3HT, it functions at a smaller extent in the case of P[(3HT)$_{1-x}$-stat-(T)$_x$] due to the smaller number of dopants intercalated in-between the side chains. Importantly, the number of the bridging-gluing centers in P[(3HT)$_{1-x}$-stat-(T)$_x$], hence the corresponding beneficial impact on the hole-mobility, increases with increasing doping level. It is then expected that at a certain doping level of P(3HT)$_{1-x}$-(T)$_x$, the two effects cross each other. This is what is indeed observed experimentally: Fig. 2**C** shows opposite trends of the conductivity values, with P3HT being the best hole conductor at a lower doping level (2.5 mol%) and P[(3HT)$_{1-x}$-stat-(T)$_x$] being the best at a larger doping level (10 mol%) outperforming the former by over 2 orders of magnitude.

Very recently, Brinkmann et al. reported the doping of mechanical rubbing aligned P3HT using different dopants such as magic blue and suggested that in highly crystalline semiconducting polymers, specifically the highly aligned ones, high charge mobilities can be achieved when the dopant is preferentially located in the amorphous phase of the polymer [72]. Herein, we show that high mobility can be achieved in doping random copolymers comprising weakly ordered connected aggregates, representing a new pathway to realize efficient charge transport, especially in the low crystalline polymers. Particularly, since many of the emerging classes of conjugated polymers are low-crystalline donor-acceptor polymers that are near-amorphous in their pristine state [73,74], it is thus important to develop an alternative route to achieve a favorable charge transport landscape.

3. Conclusion

In conclusion, we demonstrated an effective strategy allowing for significantly enhanced long-range molecular order in the doped P[(3HT)$_{1-x}$-stat-(T)$_x$] ($x \geq 0.24$) films, which overcomes the typical dopant-induced-disorder and solved the trade-off between high charge density and high charge carrier mobility in the doping of conjugated polymers. This improvement stems from additional new and unconventional roles played by the dopant molecules, which we call "bridging" and "gluing". This is due to the reduction in the density of side chains enabling the dopant to be packed closely with the polymer backbone, allowing for the establishment of a short π-π stacking distance of 3.13–3.15 Å in the doped random polymer. The "bridging" and "gluing" effects can operate instead- or in complement to the classical doping effect played by the dopant molecules. The resulting polymer-dopant-polymer supramolecular systems with ultra-tight packing allow for fast charge transfer in a higher doping load (10 mol%), resulting in remarkable improvement of charge carrier mobility and thus significantly enhanced electrical conductivity by over 100 times, compared to the doped P3HT films. This work opens up new avenues for future doping of conjugated polymers by showing that the long-range order can be simultaneously enhanced by dopants while trying to increase the charge density, holding promise for the next generation of higher-performance organic electronics. Importantly, our results clearly indicate that judicious choice of polymer structure and dopant molecules can be conceived to combine the primary destination of dopants, their redox properties, with additional properties of dopant molecules, such as bridging-gluing, allowing them to contribute in different manners to the functioning of organic electronic devices.

4. Experimental section/methods

Materials: The dopant F4TCNQ was purchased from Ossila. 2,5-Dibromothiophene, thiophene-2,5-diboronic acid bis(pinacol) ester, lithium chloride (LiCl), Tetrakis(triphenylphosphine)palladium(0) ((PPh3)4Pd(0)), Aliquat® 336 anhydrous tetrahydrofuran (THF) and anhydrous toluene were obtained from Sigma Aldrich. 2,5-Dibromo-3-hexylthiophene, 1,3-bis(diphenylphosphino)propane]nickel(II) dichloride (Ni(dppp)Cl2), 1 M isopropylmagnesium chloride (i-pro-MgCl) in THF and chlorobenzene were purchased from TCI. Methanol (MeOH), acetone, chloroform and hydrochloric acid (HCl) were purchased from VWR. The synthesis of the polymers is described in the Supporting Information.

Preparation pristine and doped polymer solutions: The polymer solutions were prepared by dissolving the polymers in chlorobenzene at concentration of 10 mg/mL. The dopant solution was prepared by dissolving F4TCNQ in chlorobenzene at a concentration of 0.5 mg/mL. All solutions were filtered through 0.45 μm filters before usage. The doped solutions were prepared by blending the two solutions according to the desired doping ratio, which was calculated as the ratio between the numbers of F4TCNQ and numbers the repeating unit of polymer semiconductors.

Film preparation and electrical measurements: Firstly, electrodes consisting of 2 nm chromium and 30 nm gold were prepared on Si substrates with 300 nm SiO_2 by photolithography and thermal evaporation techniques. Secondly, the substrate was cleaned ultrasonically in deionized water, acetone and isopropanol for 1 min each. Then, the substrate was treated by UV/ozone for 15 min. After that, the substrate was modified by octadecyltrichlorosilane (ODTS) in a vacuum oven at 120 °C for 120 min and then cleaned sequentially with chloroform, hexane and isopropanol for 1 min. Finally, the organic semiconductor solution was spin-coated on the substrate at 3000 rpm/min for 30 s prior to annealing at over 100 °C for 5 min. The bottom-gate, bottom-contact OFETs (L/W = 40 μm/1000 μm) and four-probe electrical conductivity (L/W = 160 μm/1000 μm with two fingers separated 40 μm away) were both measured using a Keithley 4200 semiconductor analyzer.

Dynamic mechanical analysis*:* Measurements were done with a Q800 from TA Instruments from −80 °C to 170 °C at a frequency of 1 Hz and a heating rate of 3 °C min^{-1} [72]. 2.5 cm × 0.5 cm pieces of a plain weave glass fiber mesh with a weight of 25 g m^{-2} (Easycomposites) were cut at an angle of 45°, drop coated with solutions comprising 10 g L^{-1} polymer dissolved in chloroform, and dried under vacuum at 60 °C for 60 min [75].

Differential scanning calorimetric analysis*:* DSC measurements were performed using a DSC instrument under N2 atmosphere at a heating and cooling rate of 10 °C/min, with a heating range of -50 − 280 °C and cooling range of 280 to −50 °C.

FTIR measurements: Infrared absorption spectra were recorded with a PerkinElmer Frontier FTIR spectrometer. The FTIR spectrum of neat FTIR was measured by sandwiching a drop of F4TCNQ dissolved in dry acetonitrile between two CaF_2 windows. FTIR spectra of doped materials were recorded for films spin-coated on cleaned CaF_2 windows.

ESR measurements: For ESR measurement, the prepared doping solution was heated and dropped on a glass substrate with a length of 5 mm and a width of 3 mm at 100 °C. Then, the glass substrate was put into the ESR tube and sealed in a glove box filled with argon gas. ESR measurement was performed at room temperature on a JEOL JES-FA200 ESR spectrometer.

Optical Characterization: Absorption spectra of pristine and doped polymer films were recorded at room using a UV−vis−NIR spectrophotometer (V-770).

Computational methods: The calculations in this study were carried out in two levels: (i) Level-1 calculations were carried out by considering dimers or complexes between two or three molecules, and (ii) Level-2 calculation were carried out by performing molecular dynamic simulations on systems containing hundreds of molecules. Detailed methods are is described in the Supporting Information.

AFM measurements: The surface morphology of polymer films was investigated by atomic force microscopy on Icon coupled at Nanoscope V controller from Bruker in the Tapping mode. The probe was a ScanAsyst Air (Bruker) with a spring constant of 0.4 N/m.

GIWAXS measurements: a laboratory setup was used (Xeuss 3.0 from Xenocs S.A.). Here, supplied with a microfocus copper source, Cu Kα radiation (wavelength (λ) = 1.5418 Å) is focused and monochromatized with a two-dimensional single reflection multilayer optic and collimated with scatterless slits. The silicon substrate surface was aligned at a grazing incident angle of 0.18° with respect to the incoming X-ray beam. The scattered X-ray were detected on an Eiger 4 M single-photon counting detector, with 75 μm pixels (DECTRIS), 80.0 mm from the sample. Conversion of the raw 2D data to reciprocal space coordinates was performed with the SimDiffraction MATLAB script package [Breiby, D. W., Bunk, O., Andreasen, J. W., Lemke, H. T. & Nielsen, M. M. (2008). J. Appl. Cryst. 41, 262−271].

Author contributions

J.K., J.G. and G.S. contributed equally to this work. J.K. synthesized the polymers; J.G. conducted electrical and ESR measurements; G.S. performed the DFT and xTB calculations; M.K.S. and J.W.A. measured and analyzed GIWAXS; K.L.W. performed MD simulations; S.P. performed AFM measurements; S.W. measured and analyzed the UV−Vis−NIR, prepared samples for GIWAXS and AFM; J.K. and M.M. recorded and analyzed the CV; S.H.K.P. and C.M. measured and analyzed FTIR, DMA and DSC; H.W. measured the OFETs of TCNQ doped polymers. J.G., Y.H. and S.W. performed overall data analysis; G.S., J.W.A., K.L.W., V.C., C.M., Y.H. and S.W. contributed to the scientific discussions and conceptualized the gluing-bridging mechanism; G.S. and S.W. wrote the manuscript with contributions from other authors. S.W. conceived and led the research.

Declaration of competing interest

The authors declare no financial interests/personal relationships which may be considered as potential competing interests.

Data availability

Data will be made available on request.

Acknowledgments

S.W. acknowledges funding from CY Initiative of Excellence (TALENT) and EUTOPIA Young Leaders Academy. Y.H thanks National Natural Science Foundation of China (62074054; U21A20497) for funding support. J.W.A acknowledges funding from the Independent Research Fund Denmark through the EPIC-OPV grant no. 1032-00326B. K.L.W. acknowledges funding from University Malaya Impact-Oriented Interdisplinary Research Grant (IIRG005A-19FNW) computation time from A*CRC Fugaku Trial for ASEAN High Performance Computing. S.H.K.P. and C. M. acknowledge funding from the Knut and Alice Wallenberg Foundation through a Wallenberg Academy Fellow Prolongation Grant. The authors thank Mr. Alexandre Michaud for NMR measurement and Ms. Marion Rollet for SEC measurement.

Appendix A. Supplementary data

Supplementary data to this article can be found online at https://doi.org/10.1016/j.mtadv.2023.100360.

References

[1] A. Salleo, Charge transport in polymeric transistors, Mater. Today 10 (2007) 38−45.
[2] A. Facchetti, π-Conjugated polymers for organic electronics and photovoltaic cell applications, Chem. Mater. 23 (2011) 733−758.
[3] X. Guo, M. Baumgarten, K. Müllen, Designing π-conjugated polymers for organic electronics, Prog. Polym. Sci. 38 (2013) 1832−1908.
[4] O. Ostroverkhova, Organic optoelectronic materials: mechanisms and applications, Chem. Rev. 116 (2016) 13279−13412.
[5] M. Ashizawa, Y. Zheng, H. Tran, Z. Bao, Intrinsically stretchable conjugated polymer semiconductors in field effect transistors, Prog. Polym. Sci. 100 (2020), 101181.
[6] S. Fratini, M. Nikolka, A. Salleo, G. Schweicher, H. Sirringhaus, Charge transport in high-mobility conjugated polymers and molecular semiconductors, Nat. Mater. 19 (2020) 491−502.
[7] A.D. Scaccabarozzi, A. Basu, F. Aniés, J. Liu, O. Zapata-Arteaga, R. Warren, Y. Firdaus, M.I. Nugraha, Y. Lin, M. Campoy-Quiles, N. Koch, C. Müller,

L. Tsetseris, M. Heeney, T.D. Anthopoulos, Doping approaches for organic semiconductors, Chem. Rev. 122 (2022) 4420–4492.
[8] M. Gross, D.C. Müller, H.-G. Nothofer, U. Scherf, D. Neher, C. Bräuchle, K. Meerholz, Improving the performance of doped π-conjugated polymers for use in organic light-emitting diodes, Nature 405 (2000) 661–665.
[9] P. Zalar, Z.B. Henson, G.C. Welch, G.C. Bazan, T.-Q. Nguyen, Color tuning in polymer light-emitting diodes with lewis acids, Angew. Chem. Int. Ed. 51 (2012) 7495–7498.
[10] C.G. Tang, M.C. Ang, K.K. Choo, V. Keerthi, J.K. Tan, M.N. Syafiqah, T. Kugler, J.H. Burroughes, R.Q. Png, L.L. Chua, P.K. Ho, Doped polymer semiconductors with ultrahigh and ultralow work functions for ohmic contacts, Nature 539 (2016) 536–540.
[11] Y. Zhang, H. Zhou, J. Seifter, L. Ying, A. Mikhailovsky, A.J. Heeger, G.C. Bazan, T.-Q. Nguyen, Molecular doping enhances photoconductivity in polymer bulk heterojunction solar cells, Adv. Mater. 25 (2013) 7038–7044.
[12] Y. Lin, Y. Firdaus, M.I. Nugraha, F. Liu, S. Karuthedath, A.-H. Emwas, W. Zhang, A. Seitkhan, M. Neophytou, H. Faber, E. Yengel, I. McCulloch, L. Tsetseris, F. Laquai, T.D. Anthopoulos, 17.1% efficient single-junction organic solar cells enabled by n-type doping of the bulk-heterojunction, Adv. Sci. 7 (2020), 1903419.
[13] G. Lu, J. Blakesley, S. Himmelberger, P. Pingel, J. Frisch, I. Lieberwirth, I. Salzmann, M. Oehzelt, R. Di Pietro, A. Salleo, N. Koch, D. Neher, Moderate doping leads to high performance of semiconductor/insulator polymer blend transistors, Nat. Commun. 4 (2013) 1588.
[14] Y. Hu, Z.D. Rengert, C. McDowell, M.J. Ford, M. Wang, A. Karki, A.T. Lill, G.C. Bazan, T.-Q. Nguyen, Doping polymer semiconductors by organic salts: toward high-performance solution-processed organic field-effect transistors, ACS Nano 12 (2018) 3938–3946.
[15] Y. Xu, H. Sun, A. Liu, H.-H. Zhu, W. Li, Y.-F. Lin, Y.-Y. Noh, Doping: a Key enabler for organic transistors, Adv. Mater. 30 (2018), 1801830.
[16] H. Wei, P.A. Chen, J. Guo, Y. Liu, X. Qiu, H. Chen, Z. Zeng, T.Q. Nguyen, Y. Hu, Low-cost nucleophilic organic bases as n-dopants for organic field-effect transistors and thermoelectric devices, Adv. Funct. Mater. (2021), 2102768.
[17] A.F. Paterson, R. Li, A. Markina, L. Tsetseris, S. MacPhee, H. Faber, A.-H. Emwas, J. Panidi, H. Bristow, A. Wadsworth, D. Baran, D. Andrienko, M. Heeney, I. McCulloch, T.D. Anthopoulos, N-Doping improves charge transport and morphology in the organic non-fullerene acceptor O-IDTBR, J. Mater. Chem. C 9 (2021) 4486–4495.
[18] Y. Liang, Z. Chen, Y. Jing, Y. Rong, A. Facchetti, Y. Yao, Heavily n-dopable pi-conjugated redox polymers with ultrafast energy storage capability, J. Am. Chem. Soc. 137 (2015) 4956–4959.
[19] R. Kroon, D.A. Mengistie, D. Kiefer, J. Hynynen, J.D. Ryan, L. Yu, C. Muller, Thermoelectric plastics: from design to synthesis, processing and structure-property relationships, Chem. Soc. Rev. 45 (2016) 6147–6164.
[20] Y. Lu, J.-Y. Wang, J. Pei, Achieving efficient n-doping of conjugated polymers by molecular dopants, Acc. Chem. Res. 54 (2021) 2871–2883.
[21] H. Guo, C.-Y. Yang, X. Zhang, A. Motta, K. Feng, Y. Xia, Y. Shi, Z. Wu, K. Yang, J. Chen, Q. Liao, Y. Tang, H. Sun, H.Y. Woo, S. Fabiano, A. Facchetti, X. Guo, Transition metal-catalysed molecular n-doping of organic semiconductors, Nature 599 (2021) 67–73.
[22] S. Wang, G. Zuo, J. Kim, H. Sirringhaus, Progress of conjugated polymers as emerging thermoelectric materials, Prog. Polym. Sci. 129 (2022), 101548.
[23] K.-H. Yim, G.L. Whiting, C.E. Murphy, J.J.M. Halls, J.H. Burroughes, R.H. Friend, J.-S. Kim, Controlling electrical properties of conjugated polymers via a solution-based p-type doping, Adv. Mater. 20 (2008) 3319–3324.
[24] A.M. Glaudell, J.E. Cochran, S.N. Patel, M.L. Chabinyc, Impact of the doping method on conductivity and thermopower in semiconducting polythiophenes, Adv. Energy Mater. 5 (2015), 1401072.
[25] E.F. Aziz, A. Vollmer, S. Eisebitt, W. Eberhardt, P. Pingel, D. Neher, N. Koch, Localized charge transfer in a molecularly doped conducting polymer, Adv. Mater. 19 (2007) 3257–3260.
[26] J. Guo, Y. Liu, P.-A. Chen, X. Wang, Y. Wang, J. Guo, X. Qiu, Z. Zeng, L. Jiang, Y. Yi, S. Watanabe, L. Liao, Y. Bai, T.-Q. Nguyen, Y. Hu, Revealing the electrophilic-attack doping mechanism for efficient and universal p-doping of organic semiconductors, Adv. Sci. 9 (2022), 2203111.
[27] H. Sirringhaus, P.J. Brown, R.H. Friend, M.M. Nielsen, K. Bechgaard, B.M.W. Langeveld-Voss, A.J.H. Spiering, R.A.J. Janssen, E.W. Meijer, P. Herwig, D.M. de Leeuw, Two-dimensional charge transport in self-organized, high-mobility conjugated polymers, Nature 401 (1999) 685–688.
[28] S. Himmelberger, K. Vandewal, Z. Fei, M. Heeney, A. Salleo, Role of molecular weight distribution on charge transport in semiconducting polymers, Macromolecules 47 (2014) 7151–7157.
[29] J. Hynynen, D. Kiefer, L. Yu, R. Kroon, R. Munir, A. Amassian, M. Kemerink, C. Muller, Enhanced electrical conductivity of molecularly p-doped poly(3-hexylthiophene) through understanding the correlation with solid-state order, Macromolecules 50 (2017) 8140–8148.
[30] E. Lim, A.M. Glaudell, R. Miller, M.L. Chabinyc, The role of ordering on the thermoelectric properties of blends of regioregular and regiorandom poly(3-hexylthiophene), Adv. Electron. Mater 5 (2019), 1800915.
[31] G. Zuo, Z. Li, O. Andersson, H. Abdalla, E. Wang, M. Kemerink, Molecular doping and trap filling in organic semiconductor host–guest systems, J. Phys. Chem. C 121 (2017) 7767–7775.
[32] P.Y. Yee, D.T. Scholes, B.J. Schwartz, S.H. Tolbert, Dopant-induced ordering of amorphous regions in regiorandom P3HT, J. Phys. Chem. Lett. 10 (2019) 4929–4934.
[33] J. Gao, E.T. Niles, J.K. Grey, Aggregates promote efficient charge transfer doping of poly(3-hexylthiophene), J. Phys. Chem. Lett. 4 (2013) 2953–2957.
[34] D.T. Scholes, S.A. Hawks, P.Y. Yee, H. Wu, J.R. Lindemuth, S.H. Tolbert, B.J. Schwartz, Overcoming film quality issues for conjugated polymers doped with F4TCNQ by solution sequential processing: Hall effect, structural, and optical measurements, J. Phys. Chem. Lett. 6 (2015) 4786–4793.
[35] I.E. Jacobs, E.W. Aasen, J.L. Oliveira, T.N. Fonseca, J.D. Roehling, J. Li, G. Zhang, M.P. Augustine, M. Mascal, A.J. Moulé, Comparison of solution-mixed and sequentially processed P3HT:F4TCNQ films: effect of doping-induced aggregation on film morphology, J. Mater. Chem. C 4 (2016) 3454–3466.
[36] D.T. Scholes, P.Y. Yee, J.R. Lindemuth, H. Kang, J. Onorato, R. Ghosh, C.K. Luscombe, F.C. Spano, S.H. Tolbert, B.J. Schwartz, The effects of crystallinity on charge transport and the structure of sequentially processed F4 TCNQ-doped conjugated polymer films, Adv. Funct. Mater. 27 (2017), 1702654.
[37] M.T. Fontana, D.A. Stanfield, D.T. Scholes, K.J. Winchell, S.H. Tolbert, B.J. Schwartz, Evaporation vs solution sequential doping of conjugated polymers: F4TCNQ doping of micrometer-thick P3HT films for thermoelectrics, J. Phys. Chem. C 123 (2019) 22711–22724.
[38] S. Wang, T.P. Ruoko, G. Wang, S. Riera-Galindo, S. Hultmark, Y. Puttisong, F. Moro, H. Yan, W.M. Chen, M. Berggren, C. Muller, S. Fabiano, Sequential doping of ladder-type conjugated polymers for thermally stable n-type organic conductors, ACS Appl. Mater. Interfaces 12 (2020) 53003–53011.
[39] A.R. Chew, R. Ghosh, Z. Shang, F.C. Spano, A. Salleo, Sequential doping reveals the importance of amorphous chain rigidity in charge transport of semi-crystalline polymers, J. Phys. Chem. Lett. 8 (2017) 4974–4980.
[40] K. Kang, S. Watanabe, K. Broch, A. Sepe, A. Brown, I. Nasrallah, M. Nikolka, Z. Fei, M. Heeney, D. Matsumoto, K. Marumoto, H. Tanaka, S. Kuroda, H. Sirringhaus, 2D coherent charge transport in highly ordered conducting polymers doped by solid state diffusion, Nat. Mater. 15 (2016) 896–902.
[41] S.N. Patel, A.M. Glaudell, K.A. Peterson, E.M. Thomas, K.A. O'Hara, E. Lim, M.L. Chabinyc, Morphology controls the thermoelectric power factor of a doped semiconducting polymer, Sci. Adv. 3 (2017), e1700434.
[42] E. Lim, K.A. Peterson, G.M. Su, M.L. Chabinyc, Thermoelectric properties of poly(3-hexylthiophene) (P3HT) doped with 2,3,5,6-Tetrafluoro-7,7,8,8-tetracyanoquinodimethane (F4TCNQ) by vapor-phase infiltration, Chem. Mater. 30 (2018) 998–1010.
[43] R. Noriega, J. Rivnay, K. Vandewal, F.P. Koch, N. Stingelin, P. Smith, M.F. Toney, A. Salleo, A general relationship between disorder, aggregation and charge transport in conjugated polymers, Nat. Mater. 12 (2013) 1038–1044.
[44] D. Venkateshvaran, M. Nikolka, A. Sadhanala, V. Lemaur, M. Zelazny, M. Kepa, M. Hurhangee, A.J. Kronemeijer, V. Pecunia, I. Nasrallah, I. Romanov, K. Broch, I. McCulloch, D. Emin, Y. Olivier, J. Cornil, D. Beljonne, H. Sirringhaus, Approaching disorder-free transport in high-mobility conjugated polymers, Nature 515 (2014) 384–388.
[45] X. Zhang, H. Bronstein, A.J. Kronemeijer, J. Smith, Y. Kim, R.J. Kline, L.J. Richter, T.D. Anthopoulos, H. Sirringhaus, K. Song, M. Heeney, W. Zhang, I. McCulloch, D.M. DeLongchamp, Molecular origin of high field-effect mobility in an indacenodithiophene-benzothiadiazole copolymer, Nat. Commun. 4 (2013) 2238.
[46] S.Y. Son, Y. Kim, J. Lee, G.Y. Lee, W.T. Park, Y.Y. Noh, C.E. Park, T. Park, High-field-effect mobility of low-crystallinity conjugated polymers with localized aggregates, J. Am. Chem. Soc. 138 (2016) 8096–8103.
[47] M. Upadhyaya, C.J. Boyle, D. Venkataraman, Z. Aksamija, Effects of disorder on thermoelectric properties of semiconducting polymers, Sci. Rep. 9 (2019) 5820.
[48] X. Yan, M. Xiong, X.-Y. Deng, K.-K. Liu, J.-T. Li, X.-Q. Wang, S. Zhang, N. Prine, Z. Zhang, W. Huang, Y. Wang, J.-Y. Wang, X. Gu, S.K. So, J. Zhu, T. Lei, Approaching disorder-tolerant semiconducting polymers, Nat. Commun. 12 (2021) 5723.
[49] Y. Lu, Z.D. Yu, H.I. Un, Z.F. Yao, H.Y. You, W. Jin, L. Li, Z.Y. Wang, B.W. Dong, S. Barlow, E. Longhi, C.A. Di, D. Zhu, J.Y. Wang, C. Silva, S.R. Marder, J. Pei, Persistent conjugated backbone and disordered lamellar packing impart polymers with efficient n-doping and high conductivities, Adv. Mater. 33 (2021), 2005946.
[50] X. Cao, H. Li, J. Hu, H. Tian, Y. Han, B. Meng, J. Liu, L. Wang, An amorphous n-type conjugated polymer with an ultra-rigid planar backbone, Angew. Chem. Int. Ed. n/a (2022), e202212979.
[51] R. Noriega, Efficient charge transport in disordered conjugated polymer microstructures, Macromol. Rapid Commun. 39 (2018), e1800096.
[52] S. Wang, Emerging efficient charge-transport landscape based on short-range order in conjugated polymers, Synth. Met. 251 (2019) 104–119.
[53] Y.M. Gross, D. Trefz, R. Tkachov, V. Untilova, M. Brinkmann, G.L. Schulz, S. Ludwigs, Tuning aggregation by regioregularity for high-performance n-type P(NDI2OD-T2) donor–acceptor copolymers, Macromolecules 50 (2017) 5353–5366.
[54] Y.M. Gross, D. Trefz, C. Dingler, D. Bauer, V. Vijayakumar, V. Untilova, L. Biniek, M. Brinkmann, S. Ludwigs, From isotropic to anisotropic conductivities in P(NDI2OD-T2) by (Electro-)Chemical doping strategies, Chem. Mater. 31 (2019) 3542–3555.
[55] S. Wang, D. Fazzi, Y. Puttisong, M.J. Jafari, Z. Chen, T. Ederth, J.W. Andreasen, W.M. Chen, A. Facchetti, S. Fabiano, Effect of backbone regiochemistry on conductivity, charge density, and polaron structure of n-doped donor-acceptor polymers, Chem. Mater. 31 (2019) 3395–3406.
[56] S. Wang, S. Fabiano, S. Himmelberger, S. Puzinas, X. Crispin, A. Salleo,

M. Berggren, Experimental evidence that short-range intermolecular aggregation is sufficient for efficient charge transport in conjugated polymers, Proc. Natl. Acad. Sci. U. S. A. 112 (2015) 10599–10604.
[57] M. Roesing, J. Howell, D. Boucher, Solubility characteristics of poly(3-hexylthiophene), J. Polym. Sci., Part B: Polym. Phys. 55 (2017) 1075–1087.
[58] H. Li, J. Song, J. Xiao, L. Wu, H.E. Katz, L. Chen, Synergistically improved molecular doping and carrier mobility by copolymerization of donor–acceptor and donor–donor building blocks for thermoelectric application, Adv. Funct. Mater. 30 (2020), 2004378.
[59] Y. Hu, Y. Gao, P. Li, X. Gao, Z. Liu, Enhancement of thermoelectric properties of D-A conjugated polymer through constructing random copolymers with more electronic donors, J. Polym. Sci. 60 (2021) 1002–1012.
[60] G. Cao, B. Li, Y. Wu, Z. Ren, X. Nie, J. Yang, J. Wu, H. Xin, L. Wang, C. Gao, Alleviating the trade-off interrelation between seebeck coefficient and electrical conductivity by random copolymerization of two-dimensional and one-dimensional monomers, Compos. Commun. 33 (2022), 101218.
[61] S. Mardi, M. Pea, A. Notargiacomo, N. Yaghoobi Nia, A. Di Carlo, A. Reale, The molecular weight dependence of thermoelectric properties of poly (3-hexylthiophene), Materials 13 (2020) 1404.
[62] D.T. Duong, C. Wang, E. Antono, M.F. Toney, A. Salleo, The chemical and structural origin of efficient p-type doping in P3HT, Org. Electron. 14 (2013) 1330–1336.
[63] P. Pingel, M. Arvind, L. Kölln, R. Steyrleuthner, F. Kraffert, J. Behrends, S. Janietz, D. Neher, p-Type doping of poly(3-hexylthiophene) with the strong lewis acid tris(pentafluorophenyl)borane, Adv. Electron. Mater 2 (2016), 1600204.
[64] H. Méndez, G. Heimel, S. Winkler, J. Frisch, A. Opitz, K. Sauer, B. Wegner, M. Oehzelt, C. Röthel, S. Duhm, D. Többens, N. Koch, I. Salzmann, Charge-transfer crystallites as molecular electrical dopants, Nat. Commun. 6 (2015) 8560.
[65] F.C. Spano, C. Silva, H- and J-aggregate behavior in polymeric semiconductors, Annu. Rev. Phys. Chem. 65 (2014) 477–500.
[66] C. Bannwarth, E. Caldeweyher, S. Ehlert, A. Hansen, P. Pracht, J. Seibert, S. Spicher, S. Grimme, Extended tight-binding quantum chemistry methods, WIREs Computational Molecular Science 11 (2021) e1493.
[67] D. Kiefer, R. Kroon, A.I. Hofmann, H. Sun, X. Liu, A. Giovannitti, D. Stegerer, A. Cano, J. Hynynen, L. Yu, Y. Zhang, D. Nai, T.F. Harrelson, M. Sommer, A.J. Moulé, M. Kemerink, S.R. Marder, I. McCulloch, M. Fahlman, S. Fabiano, C. Müller, Double doping of conjugated polymers with monomer molecular dopants, Nat. Mater. 18 (2019) 149–155.
[68] E.C.-K. Wu, C.Z. Salamat, S.H. Tolbert, B.J. Schwartz, Molecular dynamics study of the thermodynamics of integer charge transfer vs charge-transfer complex formation in doped conjugated polymers, ACS Appl. Mater. Interfaces 14 (2022) 26988–27001.
[69] J. Mei, D.H. Kim, A.L. Ayzner, M.F. Toney, Z. Bao, Siloxane-terminated solubilizing side chains: bringing conjugated polymer backbones closer and boosting hole mobilities in thin-film transistors, J. Am. Chem. Soc. 133 (2011) 20130–20133.
[70] Z.-F. Yao, J.-Y. Wang, J. Pei, High-performance polymer field-effect transistors: from the perspective of multi-level microstructures, Chem. Sci. 12 (2021) 1193–1205.
[71] Y. Huang, Z. Wang, Z. Chen, Q. Zhang, Organic cocrystals: beyond electrical conductivities and field-effect transistors (FETs), Angew. Chem. Int. Ed. 58 (2019) 9696–9711.
[72] Y. Zhong, V. Untilova, D. Muller, S. Guchait, C. Kiefer, L. Herrmann, N. Zimmermann, M. Brosset, T. Heiser, M. Brinkmann, Preferential location of dopants in the amorphous phase of oriented regioregular poly(3-hexylthiophene-2,5-diyl) films helps reach charge conductivities of 3000 S cm−1, Adv. Funct. Mater. 32 (2022), 2202075.
[73] E.H. Suh, M.-K. Jeong, K. Lee, W. Jeong, J. Jang, I.H. Jung, Solution-state doping-assisted molecular ordering and enhanced thermoelectric properties of an amorphous polymer, Int. J. Energy Res. 45 (2021) 21540–21551.
[74] E.H. Suh, M.-K. Jeong, K. Lee, W. Jeong, Y.J. Jeong, I.H. Jung, J. Jang, Understanding the solution-state doping of donor–acceptor polymers through tailored side chain engineering for thermoelectrics, Adv. Funct. Mater. 32 (2022), 2207886.
[75] S. Hultmark, S.H.K. Paleti, A. Harillo, S. Marina, F.A.A. Nugroho, Y. Liu, L.K.E. Ericsson, R. Li, J. Martín, J. Bergqvist, C. Langhammer, F. Zhang, L. Yu, M. Campoy-Quiles, E. Moons, D. Baran, C. Müller, Suppressing Co-crystallization of halogenated non-fullerene acceptors for thermally stable ternary solar cells, Adv. Funct. Mater. 30 (2020), 2005462.